Neutron Beam Effects on Spin-Exchange-Polarized ^{3}He

M. Sharma,[1] E. Babcock,[2] K. H. Andersen,[2] L. Barrón-Palos,[3,4] M. Becker,[2,5] S. Boag,[6] W. C. Chen,[7] T. E. Chupp,[1] A. Danagoulian,[8] T. R. Gentile,[7] A. Klein,[8] S. Penttila,[9] A. Petoukhov,[2] T. Soldner,[2] E. R. Tardiff,[1] T. G. Walker,[10] and W. S. Wilburn[8]

[1]*FOCUS Center and Physics Department, University of Michigan, Ann Arbor, Michigan 48104, USA*
[2]*Institut Laue-Langevin, BP 156, 38042 Grenoble Cedex 9, France*
[3]*Arizona State University, Tempe, Arizona 85287, USA*
[4]*Universidad Nacional Autónoma de México, México, D.F. 04510, México*
[5]*Physikalisches Institut, Universität Heidelberg, Philosophenweg 12, 69120 Heidelberg, Germany*
[6]*ISIS, Rutherford Appleton Labs, Chilton, Didcot OX11 0QX, United Kingdom*
[7]*National Institute of Standard and Technology, Gaithersburg, Maryland 20899-8461, USA*
[8]*Los Alamos National Lab, Los Alamos, New Mexico 87545, USA*
[9]*Oak Ridge National Lab, Oak Ridge, Tennessee 37831, USA*
[10]*University of Wisconsin, Madison, Wisconsin 53706, USA*

(Received 19 February 2008; published 20 August 2008)

We have observed depolarization effects when high intensity cold neutron beams are incident on alkali-metal spin-exchange-polarized ^{3}He cells used as neutron spin filters. This was first observed as a reduction of the maximum attainable ^{3}He polarization and was attributed to a decrease of alkali-metal polarization, which led us to directly measure alkali-metal polarization and spin relaxation over a range of neutron fluxes at Los Alamos Neutron Science Center and Institute Laue-Langevin. The data reveal a new alkali-metal spin-relaxation mechanism that approximately scales as $\sqrt{\phi_n}$, where ϕ_n is the neutron capture-flux density incident on the cell. This is consistent with an effect proportional to the concentration of electron-ion pairs but is much larger than expected from earlier work.

DOI: 10.1103/PhysRevLett.101.083002 PACS numbers: 32.80.Xx, 03.75.Be, 24.70.+s, 61.80.Hg

Polarized gaseous ^{3}He has wide application including targets and beams for nuclear physics measurements, for electron scattering studies of the structure of the neutron [1], for biomedical imaging of the airspace in the lungs [2], and as a neutron polarizer [3–5]. Each of these applications has a different set of requirements and acceptable trade-offs of polarization, density, size, and polarization stability. There are two techniques used to produce polarized ^{3}He gas: metastability exchange optical pumping (MEOP) and spin-exchange optical pumping (SEOP). MEOP polarizes pure ^{3}He at low pressure, typically 1 mbar, at rates of about 1 bar-l/h with ^{3}He polarizations of 70% or more [5]. MEOP polarizer stations compress the ^{3}He into cells that are transported to the point of use, where the ^{3}He polarization decays very slowly, with a time constant that can be a week or longer [6]. For SEOP, the ^{3}He is polarized by the hyperfine interaction during collisions of the ^{3}He nuclei with polarized valence electrons of optically pumped alkali metals. Production rates with SEOP are about an order of magnitude lower than the highest MEOP rates, but similarly high ^{3}He polarizations have been achieved [7]. For applications that require several days or weeks of stable high polarization operation, such as targets for electron scattering, neutron scattering instruments with limited access, and long-running fundamental neutron physics experiments, it is practical to have a SEOP system pumping continuously, with stable polarization, for weeks or months [4,8].

Gaseous polarized ^{3}He is used for polarized neutron measurements because of the nearly complete spin dependence of the absorption cross section for the process $^3\mathrm{He}(n, p)^3\mathrm{H}$. This proceeds through an unbound 0^+ resonance in ^{4}He, so that only neutrons with spin opposite to the ^{3}He spin are absorbed [9]. For neutrons incident on a cell with ^{3}He polarization P_3, the effective absorption cross section is proportional to the wavelength λ and proportional to $(1 - P_3)$ for neutron spin parallel and to $(1 + P_3)$ for neutron spin antiparallel to the ^{3}He spin. In a spin-filter polarizer, the ^{3}He polarization is not complete, and neutrons of both spin states are absorbed, though with different absorption lengths. The resulting neutron polarization is $P_n(\lambda) = \tanh(P_3\sigma_0 t_3 \frac{\lambda}{\lambda_0})$, where $\sigma_0 = 5333 \pm 7$ b is the absorption cross section for thermal neutrons ($\lambda_0 = 1.8$ Å) [10] and t_3 is the ^{3}He areal density. Transmission of polarized neutrons through polarized ^{3}He can also be used as a neutron polarization analyzer.

In a typical SEOP neutron spin filter, the ^{3}He cells are constructed from boron-free-aluminosilicate glass [11]. The alkali metal (rubidium [12] or a mixture of rubidium and potassium [13]) is distilled into the cell with about one bar of ^{3}He at room temperature and a small amount of N_2 added to suppress radiation trapping, the multiple scattering of optical-pumping photons that depolarize the alkali-metal atoms [14]. The cell is heated to maintain an optimum alkali-metal vapor pressure, held in a magnetic field of 1–3 mT, and illuminated by a high powered laser tuned

to the rubidium $D1$ resonance at 794.7 nm. The ^{3}He polarization is governed by an exponential time dependence with rate constant and equilibrium polarization given, respectively, by

$$\Gamma = (1 + X_{\text{cell}})\gamma_{\text{SE}} + \Gamma_R, \qquad P_3^{\text{eq}} = P_A \frac{\gamma_{\text{SE}}}{\Gamma}, \quad (1)$$

where $\gamma_{\text{SE}} = \langle \sigma_{\text{SE}} v \rangle [\text{Rb}]$, the velocity-averaged spin-exchange rate constant, is typically $1/(10\text{–}15\ \text{h})$. The ^{3}He relaxation rate Γ_R is a sum of rates due to cell wall interactions, impurities, ^{3}He dipole-dipole relaxation, magnetic field gradients, and ionization effects. The rate Γ_R is generally 10–50 times smaller than γ_{SE}. The volume-averaged alkali-metal electron polarization is P_A, and the factor X_{cell} accounts for an observed reduction in ^{3}He polarization that varies from cell to cell [15].

Neutron-beam effects on the ^{3}He polarization were first observed during development of the NPDGamma experiment at the Los Alamos Neutron Science Center (LANSCE) [4,16] and were further studied in dedicated runs at LANSCE and at the Institute Laue-Langevin (ILL) in Grenoble. The ^{3}He polarization for a cell used at LANSCE over two months is shown in Fig. 1. The cells and setup are described in Ref. [4]. The top panel in Fig. 1 shows that, though the ^{3}He polarization appears relatively constant over the long term (except for the period with the laser off), there is a slow downward drift. The long time constant decay of ^{3}He polarization appears to be due to a milky white coating that builds up on the cell walls and

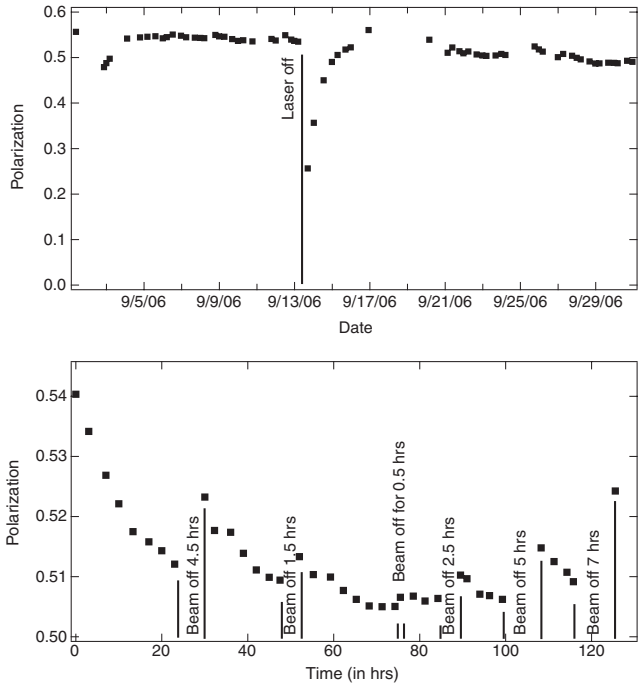

FIG. 1. LANSCE neutron spin filter ^{3}He polarization. The top panel shows the long term behavior; the bottom panel shows the effect of the neutron beam on short time scales.

reduces transmission of laser light into the cell [4]. This buildup is probably due to rubidium compounds, possibly due to reaction with the hydrogen (^{1}H and ^{3}H) produced by neutron absorption on ^{3}He. A similar effect was observed for a pure rubidium cell at 170 °C placed in the full flux PF1B beam at ILL for 1 h. Exposure for 1 h at PF1B is equivalent to about 4 days at LANSCE FP12. A Monte Carlo calculation based on the measured brightness of the LANSCE neutron source [17] predicts a maximum capture-flux density of $(1\text{–}3) \times 10^8\ \text{cm}^{-2}\,\text{s}^{-1}$. (Capture flux, the integral of the $1/v$ weighted neutron intensity spectrum, is proportional to the total neutron capture or decay rate per unit length.) The PF1B capture-flux density at the cell position was measured with gold foil activation and found to be $1.4 \times 10^{10}\ \text{cm}^{-2}\,\text{s}^{-1}$. The PF1B beam is described in Ref. [18]

Data for P_3 on shorter time scales are shown in the bottom panel in Fig. 1. When the beam is on, the ^{3}He polarization decays, and with the beam off, the polarization recovers, at least partially. The short time-scale data of Fig. 1 show that the neutron beam causes the ^{3}He polarization to decay to a lower value of P_3^{eq} at a rate of approximately $1/12$ h, which is consistent with the measured Γ. The polarization was not measured with the neutron beam off, because we used the neutrons to measure P_3 [4]; however, the increase of ^{3}He polarization is consistent with a similar rate constant. Subsequent measurements at ILL also showed a neutron-beam-induced drop in ^{3}He polarization with similar magnitude and time dependence. Since Γ does not change appreciably, the most likely cause is a drop of P_A, possibly due to ionization effects induced by the neutron-beam. Ionization effects on both Γ and P_A were observed in work with a 180 particle-nA beam of 18 MeV α particles [19]. Those observations led to the development of the double cell now ubiquitous in SEOP-based polarized ^{3}He targets for electron scattering [20]; however, we expected these effects to be negligible for ^{3}He cells in neutron beams, where the ionization energy loss is 100–10 000 times less at ILL and LANSCE, respectively. We therefore set out to measure the effects of the neutron beam on the alkali-metal polarization in high-flux neutron beams under a range of conditions.

The volume-averaged alkali-metal polarization was directly measured using electron-spin resonance (ESR) at both LANSCE and ILL. In the LANSCE setup, the transmission of optical-pumping light from a single 30 W broadband laser-diode array was monitored as rf at 14 MHz was applied and the magnetic field swept from 2.84 to 2.90 mT. The magnetic field was produced by the combination of a very uniform 1 mT field from a large set of coils and a pair of hand-wound rectangular coils that produced a less homogeneous field of about 2 mT. The consequence of the inhomogeneity is that the ESR lines are broadened, and the hyperfine lines are not all separately resolved. Data for ^{85}Rb ($I = 5/2$) for two different

neutron-beam intensities and no beam are shown in Fig. 2. When the hyperfine levels are not resolved, the rubidium polarization is given by $P_A = (7R - 3)/(7R + 3)$ for $I = 5/2$ and $P_A = (2R - 1)/(2R + 1)$ for $I = 3/2$. Here R is the ratio of adjacent ESR peak areas extrapolated to zero rf power [21].

For the ILL setup, the ESR measurements used a hybrid Rb-K cell constructed at National Institute of Standard and Technology [7]. The cell was illuminated by light from two 100-W narrowed diode-laser-array bars [22]. A linearly polarized probe laser, tuned near the Rb $D2$ resonance and directed along the magnetic field, was used to measure the Faraday rotation signal, which is proportional to the alkali-metal polarization [23]. The magnetic field was set at 1 mT, and the frequency of the rf field was swept across the $I = 3/2$ resonances. The second-order Zeeman splitting of potassium is much larger than that of rubidium and allows the separate ESR lines in ^{39}K to be resolved as shown in Fig. 3. Because of rapid spin exchange between the rubidium and potassium [24], the ESR of ^{39}K measures the average electron polarization of all of the alkali-metal species. Signals from ^{87}Rb and ^{41}K [13] are also observed; however, the ^{87}Rb transitions are not separately resolved at 1 mT.

The alkali-metal polarization at any position in the cell is given by [12]

$$\frac{1}{P_A(\vec{r})} = 1 + \frac{\Gamma_{\mathrm{SD}}}{\gamma_{\mathrm{opt}}(\vec{r})}, \tag{2}$$

where $\gamma_{\mathrm{opt}}(\vec{r})$ is the convolution of the laser spectral profile and the optical absorption cross section at the position $\vec{r}$. The spin destruction rate Γ_{SD} is the rate of electron spin flips per alkali-metal atom and is most likely affected by the neutron beam more significantly than $\gamma_{\mathrm{opt}}(\vec{r})$. In Fig. 4, we plot the change $\Delta(1/P_A)$ relative to no beam as a function of neutron capture-flux density ϕ_n for both the LANSCE and the ILL data. With the higher power narrowed lasers pumping the hybrid cell at ILL, γ_{opt} was much larger, and the neutron-beam effects are significantly less than observed at LANSCE for a given neutron-flux density.

Relaxation of the alkali-metal polarization was studied at ILL using the relaxation in the dark technique [25]. A small alkali-metal polarization was produced by a low power optical-pumping beam (less than 0.1 W/cm^2), which was chopped at 1 Hz. The polarization P_A was measured by Faraday rotation with the same setup used for the data shown in Fig. 3. With the optical-pumping beam chopped off, the polarization decayed at a rate $\Gamma_A = \Gamma_{\mathrm{SD}}/S$, where the slowing factor $S \geq 1$ accounts for the angular momentum stored in the nuclear spins, which couple to the electron spin through the hyperfine interaction [26]. Because of electron spin exchange, the factor S is an average over isotopes and alkali-metal species. The slowing factor depends on the alkali-metal polarization; for low polarization, $S = 10.8$ for natural rubidium [26], and $S = 6$ for potassium [13]. Results for $\Delta\Gamma_A$, the neutron-flux contribution to the relaxation rate, for five cells with different gas and alkali-metal compositions are shown in Fig. 5. With no beam, Γ_A varies from 20 to 30 s^{-1} depending on gas and alkali-metal compositions and pressures. The solid line in Fig. 5 has the form $\Delta\Gamma_A \propto \sqrt{\phi_n}$. As shown below, this would be consistent with relaxation due to a recombination-limited equilibrium electron or ion concentration.

The processes due to the 764 keV deposited by the ^{3}He$(n, p)^3$H reaction are complex and involve ions, metastable ^{3}He atoms, molecular ions, and radicals of helium and nitrogen. One or more of these species may be the cause of the observed effects. We consider the simplified

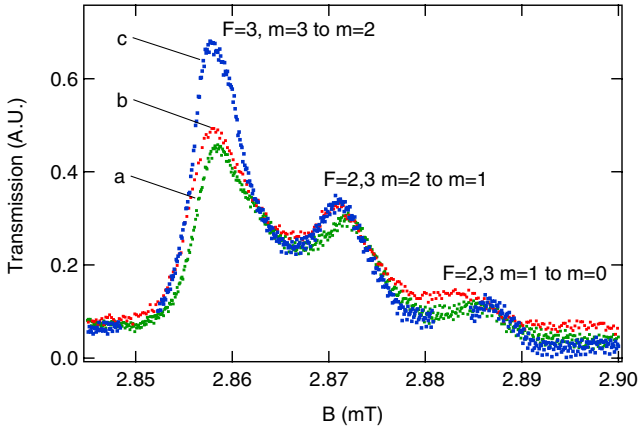

FIG. 2 (color online). ESR spectra of ^{85}Rb for full flux [(a): green] and 19% of full flux [(b): red] and no beam [(c): blue] at LANSCE. The polarizations are $P_A = 0.78$, 0.81, and 0.90, respectively. The relative uncertainties, estimated to be 1%–2%, are limited by the signal-to-noise ratio of the ESR measurements.

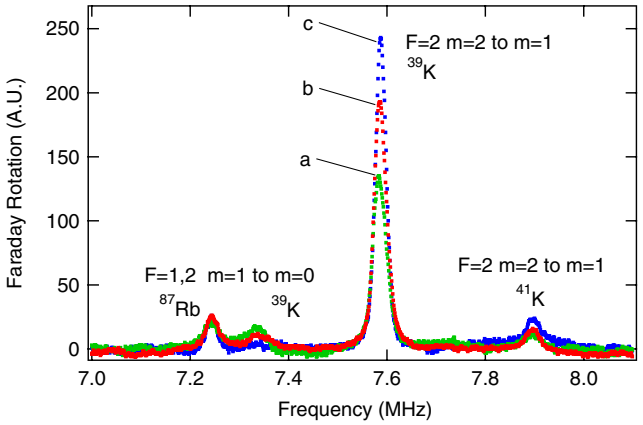

FIG. 3 (color online). ESR spectra of ^{39,41}K and ^{87}Rb for full flux [(a): green] and 8.5% of full flux [(b): red] and no flux [(c): blue] at ILL. The polarizations are $P_A = 0.83$, 0.90, and 0.98, respectively.

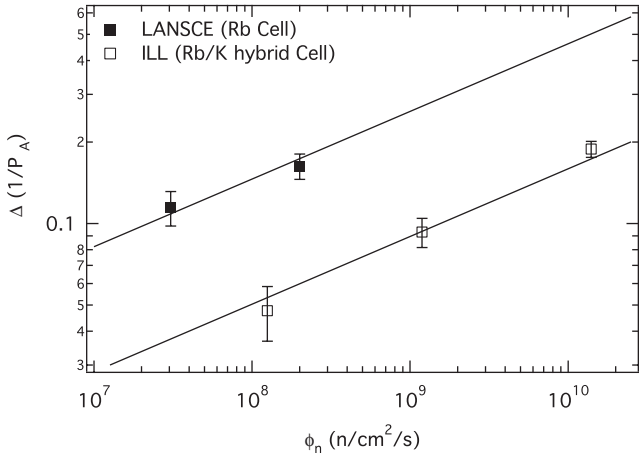

FIG. 4. Neutron-induced change in alkali-metal polarization for the LANSCE Rb cell and the ILL hybrid cell. The solid lines are provided to guide the eye.

case of spin destruction due to electrons or ions so that $\Delta\Gamma_A = k_e n_e + \sum_s k_s n_s$, where the k's are rate constants for relaxation due to each species, n_e is the electron density, and $n_s = f_s n_e$ is the density of an ion species, which is a fraction f_s of the electron density. Each f_s is, in general, a function of n_e, and $\sum_s f_s = 1$ for singly ionized species. We expect that electron-ion pairs are produced at a rate proportional to the neutron capture-flux density ϕ_n, and the rate equation for the electron density is $\frac{dn_e}{dt} = \sum_i \gamma_i \phi_n - n_e \sum_j \alpha_j n_j$, where $\gamma_i = (764\ \mathrm{keV}/E_i)/L$ for a cell of length L, E_i is the energy required to form an ion pair for each species (e.g., $E_i = 42.3$ and 32.6 eV, respectively, for helium and N_2), and the α's are the recombination coefficients for each species. If there is a single dominant species, the equilibrium electron concentration becomes $n_e \approx \sqrt{\phi_n(\sum_i \gamma_i/\alpha)}$, and $\Delta\Gamma_A \propto \sqrt{\phi_n}$. The experimental results in Fig. 5 show that the neutron-beam-induced relaxation rate does scale closely with $\sqrt{\phi_n}$, strongly suggesting that the observed spin relaxation is due to collisions with electrons or ions.

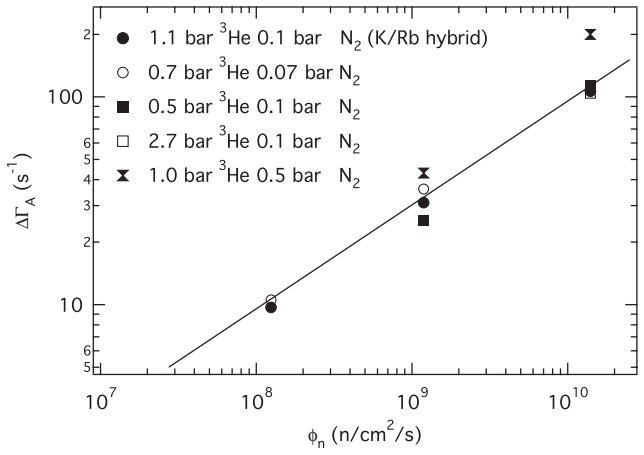

FIG. 5. ILL alkali-metal polarization relaxation results for all cells. Error bars of $\approx 10\%$ are similar to the size of the symbols. The solid line, provided to guide the eye, is proportional to $\sqrt{\phi_n}$.

In summary, measurements with *in situ* SEOP ^{3}He neutron spin filters at LANSCE and ILL have shown that the incident neutron beam induces an increase of the alkali-metal relaxation rate and a corresponding decrease of alkali-metal and ^{3}He polarization. As shown in Fig. 1, the full neutron flux at LANSCE reduced P_3^{eq} by about 5%–10%, and the subsequent measurement of P_A showed a similar reduction. With the full ILL PF1B flux, P_A was reduced by about 20% in a potassium-rubidium hybrid cell pumped by high-power narrowed diode laser arrays. The drop in ^{3}He polarization for the hybrid cell was also observed to be consistent with the drop in P_A. The magnitude of these effects is much larger than expected given earlier study of ionization effects produced by an α-particle beam [19]. Measurements over several decades of neutron flux show that the increased spin-relaxation rate approximately scales with $\sqrt{\phi_n}$, which would be consistent with the recombination-limited equilibrium concentration of electrons or ions. Further neutron-beam-related effects were observed in the ILL measurements including a combination of prompt and delayed changes in the alkali-metal relaxation rates, cell pressure-dependent effects, and performance of a double cell. These will be presented in a separate paper.

This work was supported by the U.S. National Science Foundation, the Department of Energy, the ILL Millennium Program, and the NMI3. We gratefully acknowledge the efforts of the entire NPDGamma Collaboration in developing the apparatus used to provide the data shown in Fig. 1, and we gratefully acknowledge the technical assistance of the ILL ^{3}He group.

[1] T. Chupp *et al.*, Annu. Rev. Nucl. Part. Sci. **44**, 373 (1994).
[2] H. U. Kauczor *et al.*, European Radiology **8**, 820 (1998).
[3] K. P. Coulter *et al.*, Nucl. Instrum. Methods Phys. Res., Sect. A **288**, 463 (1990).
[4] T. E. Chupp *et al.*, Nucl. Instrum. Methods Phys. Res., Sect. A **574**, 500 (2007).
[5] A. Petoukhov *et al.*, Physica (Amsterdam) **385B–386B**, 1146 (2006).
[6] K. H. Andersen *et al.*, Physica (Amsterdam) **385B–386B**, 1134 (2006).
[7] W. C. Chen, T. R. Gentile, T. G. Walker, and E. Babcock, Phys. Rev. A **75**, 013416 (2007).
[8] J. R. Johnson *et al.*, Nucl. Instrum. Methods Phys. Res., Sect. A **356**, 148 (1995).
[9] L. Passell and R. I. Schermer, Phys. Rev. **150**, 146 (1966).
[10] S. F. Mughabghab *et al.*, *Neutron Cross Sections* (Academic, New York, 1981).
[11] G. L. Jones *et al.*, Nucl. Instrum. Methods Phys. Res., Sect. A **440**, 772 (2000).
[12] T. E. Chupp *et al.*, Phys. Rev. C **36**, 2244 (1987).
[13] E. Babcock *et al.*, Phys. Rev. Lett. **91**, 123003 (2003).

[14] T. E. Chupp and K. P. Coulter, Phys. Rev. Lett. **55**, 1074 (1985).
[15] E. Babcock *et al.*, Phys. Rev. Lett. **96**, 083003 (2006).
[16] M. Gericke *et al.*, Phys. Rev. C **74**, 065503 (2006).
[17] P. Seo *et al.*, Nucl. Instrum. Methods Phys. Res., Sect. A **517**, 285 (2004).
[18] H. Abele *et al.*, Nucl. Instrum. Methods Phys. Res., Sect. A **562**, 407 (2006).
[19] K. P. Coulter *et al.*, Nucl. Instrum. Methods Phys. Res., Sect. A **276**, 29 (1989).
[20] T. E. Chupp *et al.*, Phys. Rev. C **45**, 915 (1992).
[21] E. Babcock *et al.*, Phys. Rev. A **71**, 013414 (2005).
[22] B. Chann *et al.*, J. Appl. Phys. **94**, 6908 (2003).
[23] E. Vliegen *et al.*, Nucl. Instrum. Methods Phys. Res., Sect. A **460**, 444 (2001).
[24] L. W. Anderson *et al.*, Phys. Rev. **120**, 1279 (1960).
[25] W. Franzen, Phys. Rev. **115**, 850 (1959).
[26] M. E. Wagshul and T. E. Chupp, Phys. Rev. A **49**, 3854 (1994).